International Journal of Scientific Research in Engineering and Management (IJSREM)
Volume: 10 Issue: 10 | Oct - 2026 SJIF Rating: 8.659 ISSN: 2582-3930

Uncertainty-Aware Simulation of Adaptive Charging for Electric Vehicle Batteries under Ultra-Fast Charging Conditions

K Lakshmi Prasad Reddy[1*], and M. Vijaya Kumar[2]

[1]Research Scholar in department of EEE, JNTU College of Engineering, Anantapur, Andhra Pradesh, India
[1]Lecturer in Department of EEE, Government Polytechnic, Jammalamadugu, Andhra Pradesh, India
[2]Professor in department of EEE, JNTU College of Engineering, Anantapur, Andhra Pradesh, India

---

Abstract - Ultra-fast charging is an important requirement for electric vehicles, but increasing charging current can intensify battery heating and create challenges for thermal management. This paper presents a simulation-based investigation of adaptive charging compared with a constant-current baseline under electrical and thermal parameter uncertainty. Four battery-chemistry configurations are considered: lithium iron phosphate (LFP), nickel manganese cobalt oxide (NMC), nickel cobalt aluminum oxide (NCA), and a projected solid-state configuration. A reduced-order electro-thermal model is implemented using a nominal battery capacity of 60 Ah and a 15-minute charging interval. The adaptive controller reduces the charging current progressively after the state of charge reaches 80%, while the baseline maintains the prescribed current limit. A paired Monte Carlo analysis with 1,000 parameter samples examines the effects of variations in electrical resistance, effective thermal capacity, and cooling coefficient. Under the selected nominal assumptions, the simulated maximum temperature rise for NMC decreases from approximately 5.80°C to 5.15°C, while the corresponding value for NCA decreases from approximately 5.29°C to 4.68°C. These reductions are accompanied by changes in the energy delivered during the charging interval. The LFP configuration exhibits no difference between the two strategies because the simulated state of charge does not reach the adaptive controller's activation threshold. The results demonstrate how charging-control decisions and assumed model parameters influence predicted thermal behaviour. Since the model has not been calibrated against experimental measurements, the findings are limited to exploratory simulation comparisons and do not establish actual battery degradation, lifetime extension, or safety improvements.

Key Words: Adaptive charging, electric vehicles, electro-thermal modelling, Monte Carlo simulation, parameter uncertainty, ultra-fast charging, battery thermal response.

1. INTRODUCTION

The growing adoption of electric vehicles (EVs) has increased the demand for charging systems capable of transferring energy within shorter periods. Ultra-fast charging is a promising approach for reducing charging time and improving the convenience of EV operation [1-3]. However, the use of high charging currents introduces thermal-management challenges because the heat generated within a battery depends on its electrical characteristics and operating conditions. Consequently, the development of suitable charging strategies requires consideration of both charging performance and the battery's thermal response.

Battery temperature during charging is influenced by several factors, including internal electrical resistance, charging current, ambient temperature, thermal capacity, and heat dissipation. These factors can vary with battery chemistry, design, operating conditions, and cooling arrangements. Therefore, a charging strategy that produces favourable results under one set of assumed parameters may behave differently when those parameters change [4,5]. Evaluating charging strategies under parameter uncertainty is important for understanding the reliability and limitations of simulation-based performance comparisons.

Constant-current charging provides a useful reference for assessing alternative charging-control methods. Under this approach, the charging current is maintained at a prescribed level, subject to the constraints represented in the model. Adaptive charging, in contrast, modifies the current according to selected operating conditions, such as state of charge. Reducing the charging current during part of the charging process may lower the predicted thermal response, but it can also reduce the energy delivered within a fixed charging interval [6,7]. Therefore, an appropriate comparison should consider thermal indicators alongside energy delivery and final state of charge rather than evaluating the controller using a single performance measure.

The choice of battery chemistry also influences the outcome of such comparisons. Lithium iron phosphate (LFP), nickel manganese cobalt oxide (NMC), and nickel cobalt aluminum oxide (NCA) batteries can be represented using chemistry-specific electrical parameters and charging-current limits. Solid-state batteries may also be included in comparative simulation studies; however, their model parameters must be distinguished from experimentally measured properties when projected values are used. Accordingly, comparisons across these configurations should account for the assumptions underlying each parameter set and avoid interpreting simulated rankings as universal characteristics of the respective battery technologies [8-11].

Reduced-order electro-thermal models offer a computationally efficient means of examining the relationship between charging current and temperature. Nevertheless, predictions from these models depend on the selected parameter values and the simplifications introduced in their formulation. Electrical resistance affects the calculated heat generation, whereas effective thermal capacity and cooling characteristics influence the predicted temperature trajectory. A study based only on nominal parameter values may not adequately reveal how sensitive the results are to uncertainty in these quantities. Monte Carlo simulation provides a practical framework for investigating this sensitivity by repeatedly evaluating the model using different parameter combinations [12,13].

Although simulation can support systematic comparisons, uncertainty analysis alone does not establish the accuracy of a

model for a physical battery. The results depend on the model structure, parameter ranges, controller definition, and initial conditions. Experimental measurements or an independently validated reference model are required before the predicted thermal behaviour can be treated as representative of an actual battery system. In addition, a lower predicted temperature rise should not automatically be interpreted as reduced battery degradation, because degradation depends on mechanisms that are not represented explicitly by a simple thermal model [14,15].

Research motivation and contribution: In view of these considerations, this study investigates the simulated thermal response of adaptive charging relative to a constant-current baseline under selected electrical and thermal parameter variations. A reduced-order electro-thermal model is applied to four battery-chemistry parameter sets over a fixed charging interval. Paired Monte Carlo simulations use the same sampled parameter values for both charging strategies, allowing their predicted responses to be compared under consistent conditions. The analysis considers maximum temperature rise, energy delivered, final state of charge, and a temperature-based stress index.

The main contributions of this paper are threefold. First, it establishes a reproducible simulation framework for comparing adaptive and constant-current charging under a common set of operating assumptions. Second, it evaluates the sensitivity of the predicted thermal response to variations in electrical resistance, effective thermal capacity, and cooling coefficient using paired Monte Carlo simulations. Third, it examines the relationship between the predicted thermal response and energy delivery across the selected battery-chemistry configurations, while explicitly identifying the limitations associated with assumed parameters and the absence of experimental calibration.

The findings are intended to provide an exploratory assessment of adaptive charging under parameter uncertainty rather than a definitive evaluation of battery lifetime or safety. By reporting the controller assumptions, uncertainty bounds, and limitations alongside the numerical results, the study aims to support transparent interpretation and further development of simulation-based charging assessments.

The remainder of this paper is organized as follows. Section-2 describes the battery parameter sets, charging strategies, electro-thermal model, and uncertainty-analysis procedure. Section-3 presents the nominal simulation results and paired Monte Carlo comparisons. Section-4 discusses the implications and limitations of the findings, and Section-5 concludes the paper and outlines directions for further validation.

2. SYSTEM MATHEMATICAL FORMULATION

2.1. System Configuration and Modelling Assumptions

The proposed study employs a reduced-order electro-thermal model to investigate the response of electric vehicle (EV) batteries under adaptive and constant-current charging. The model represents the interaction between charging current, state of charge (SoC), resistive heat generation, and heat dissipation. Four battery-chemistry configurations are considered: lithium iron phosphate (LFP), nickel manganese cobalt oxide (NMC), nickel cobalt aluminum oxide (NCA), and a projected solid-state battery configuration.

Fig. 1 illustrates input parameters, charging strategy selection, the electro-thermal battery model, performance indicators, Monte Carlo uncertainty analysis, and statistical comparison.

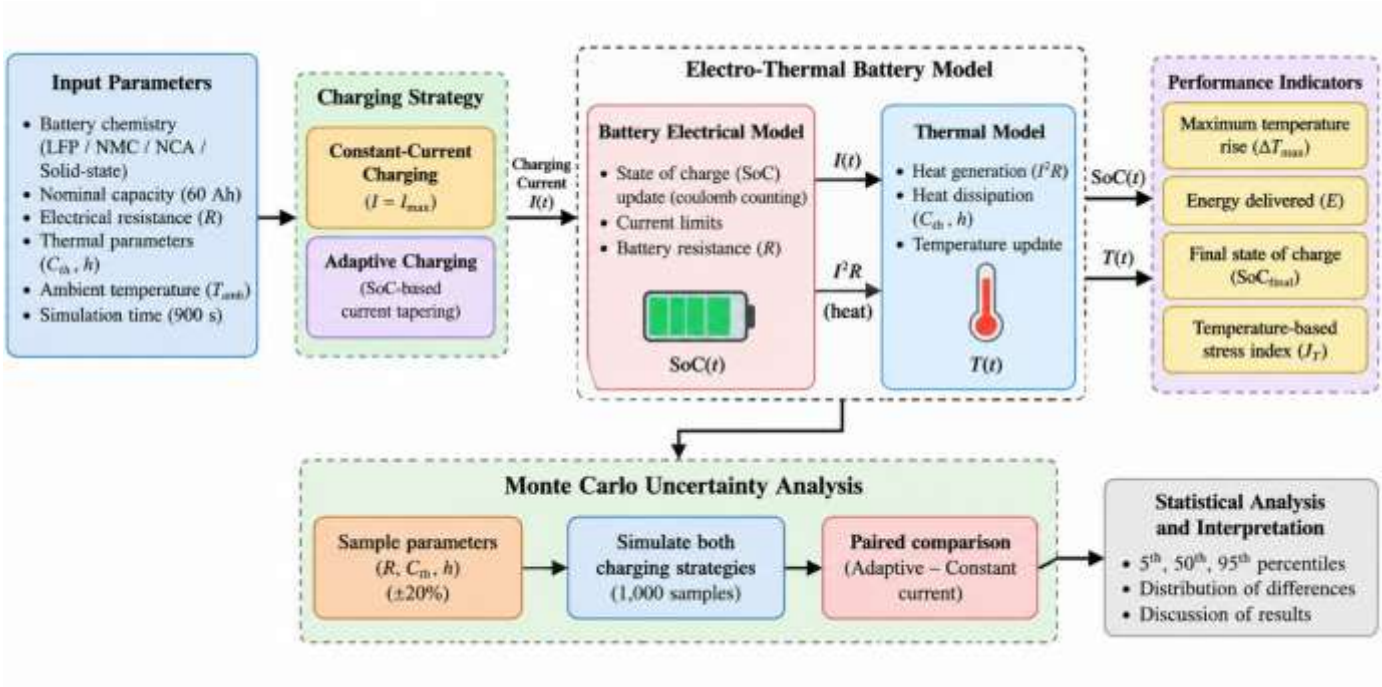


Fig-1: Block diagram of the proposed system

The nominal battery capacity is set to 60 Ah, and the charging process is simulated over a fixed duration of 900 s with a time step of 1 s. The ambient temperature is maintained at 25°C. The chemistry-dependent resistance and maximum C-rate values adopted as model inputs are presented in Table 1, whereas the effective thermal capacity, cooling coefficient, constant pack voltage, and adaptive controller thresholds are treated as modelling assumptions.

Table-1. Parameters used in the simulation model

Parameter	Value
Nominal battery capacity	60 Ah
Simulation duration	900 s
Simulation time step	1 s
Ambient temperature	25°C
Assumed constant pack voltage	833.3 V
Assumed effective thermal capacity	20,000 J/K
Assumed cooling coefficient	5 W/K
Adaptive taper initiation	80% SoC
Adaptive taper completion	95% SoC
Assumed terminal charging rate	1.5C
Monte Carlo samples	1,000
Parameter variation	±20% of nominal values

The nominal electrical resistance and maximum C-rate differ among the four configurations. For LFP, NMC, NCA, and the projected solid-state configuration, the resistance values are 0.0030 Ω, 0.0025 Ω, 0.0020 Ω, and 0.0015 Ω, respectively. The corresponding maximum C-rates are 3C, 4C, 4.5C, and 5C. These values are treated as prescribed simulation inputs rather than experimentally verified characteristics of specific commercial batteries.

The solid-state configuration is included as a projected parameter scenario. Its simulated response is therefore not interpreted as evidence of experimentally demonstrated solid-state battery performance.

2.2. State-of-Charge Model

The battery state of charge is represented by a discrete-time coulomb-counting equation. Let (z_k) denote the normalized SoC at time step (k), (I_k) the charging current in amperes, (Q) the nominal capacity in ampere-hours, and (Δt) the time step in seconds. The SoC update is expressed as in Eq. (1).

$$z_{k+1} = \min\left[1, z_k + \frac{I_k \Delta t}{3600Q}\right] \quad (1)$$

The initial SoC is set to zero. The charging current is constrained so that the simulated SoC does not exceed unity. Once the SoC reaches 100%, the commanded current is set to zero.

Eq. (1) represents idealized coulomb counting. It does not explicitly account for coulombic efficiency, capacity variation with temperature, self-discharge, or state-of-charge estimation error. These effects are outside the scope of the present simplified model.

2.3. Charging-Current Formulation

Two charging strategies are investigated: a constant-current baseline and an adaptive charging strategy. Both are evaluated using the same nominal battery parameters and simulation duration.

1) Constant-current baseline

The maximum prescribed charging current for each configuration is calculated from its nominal capacity and maximum C-rate is given in Eq. (2).

$$I_{max} = C_{\text{rate,max}} Q \quad (2)$$

where $C_{rate,max}$ is the assumed maximum C-rate expressed in reciprocal hours.

The current is additionally limited to prevent the discrete-time SoC update from exceeding 100%. This baseline is an idealized constant-current reference rather than a complete representation of a practical constant-current/constant-voltage charging protocol.

2) Adaptive charging strategy

The adaptive strategy maintains the prescribed maximum current while the SoC is below 80%. When the SoC enters the interval from 80% to 95%, the current is reduced linearly toward an assumed terminal current of 1.5C. The commanded current is defined as in Eq. (3).

$$I_k^{AD} = I_{max}, \quad z_k < z_s;$$

$$= I_{max} + \frac{z_k - z_s}{z_e - z_s}(I_t - I_{max}), \quad z_s \le z_k < z_e;$$

$$= I_t, \quad z_k \ge z_e \quad (3)$$

where (z_s=0.80) is the taper-start SoC, (z_e=0.95) is the taper-end SoC, and (I_t=1.5Q) is the assumed terminal current in amperes. The current is set to zero after the model reaches full SoC and is constrained by the remaining charge required to reach that limit.

Eq. (3) defines a prescribed SoC-dependent current schedule. It is not an optimization-based controller, and the taper thresholds and terminal current have not been established through experimental optimization. The resulting comparison therefore evaluates this particular adaptive schedule rather than adaptive charging in general.

2.4. Reduced-Order Electro-Thermal Model

The thermal behaviour is represented using a single lumped-temperature state. The model assumes that the battery can be described by an effective thermal capacity and an effective heat-transfer coefficient. Resistive heating is the only internal heat-generation mechanism explicitly included. The governing thermal equation is given in Eq. (4).

$$C_{th}\frac{dT}{dt} = I^2R - h(T - T_{amb}) \quad (4)$$

where (T) is the modelled battery temperature in degrees Celsius, (C_{th}) is the effective thermal capacity in J/K, (R) is the electrical resistance in ohms, (h) is the effective cooling coefficient in W/K, and (T_{amb}) is the ambient temperature. The term (I^2R) represents resistive heat generation, while (h(T-

T_{amb})) represents heat removal to the surrounding environment.

The initial battery temperature is set equal to the ambient temperature. The implementation prevents the calculated temperature from falling below ambient temperature.

The model uses nominal values of (C_{th}=20,000) J/K and (h=5) W/K. These are assumed effective parameters, not calibrated measurements. The formulation also neglects spatial temperature gradients, reversible electrochemical heat, temperature-dependent resistance, and detailed cooling-system dynamics. Accordingly, the calculated temperature is interpreted as a modelled lumped thermal response rather than a prediction of the hottest location within a physical battery pack.

2.5. Monte Carlo Parameter-Uncertainty Analysis

The sensitivity of the simulated results to parameter uncertainty is investigated using a paired Monte Carlo procedure. For each sample, the electrical resistance, effective thermal capacity, and cooling coefficient are independently varied within ±20% of their nominal values. Uniform distributions are used for these variations, and the same sampled values are applied to the adaptive and constant-current simulations within each paired comparison.

The 5th, 50th, and 95th percentiles of the simulated indicators and paired differences are used to summarize their distributions. The proportion of samples for which (ΔTmax<0) is also calculated to describe how frequently adaptive charging produces a lower peak temperature within the selected model and uncertainty bounds.

The ±20% parameter variations are exploratory assumptions rather than empirically established probability distributions. Therefore, the resulting percentiles and sample frequencies characterize uncertainty within the prescribed model and parameter ranges; they should not be interpreted as confidence intervals for real battery performance or as probabilities of real-world success.

The proposed formulation provides a computationally simple framework for examining how a prescribed adaptive charging schedule affects the predicted thermal response under selected parameter variations. Its main advantage is that both charging strategies can be evaluated under matched conditions, allowing differences in the model outputs to be attributed to the prescribed current schedules within the stated assumptions.

Several limitations must be recognized. First, the use of a constant pack voltage simplifies energy calculation and does not capture a realistic voltage-versus-SoC relationship. Second, the lumped thermal model uses assumed effective thermal parameters and includes only resistive heat generation and linear heat dissipation. Third, the C-rate limits and resistance values are prescribed inputs that require traceable justification for the battery representation being studied. Finally, no experimental calibration or independent validation is included in the present model.

These limitations define the interpretation of the subsequent results. The study compares simulated responses under specified assumptions and does not establish experimental charging performance, battery degradation reduction, or safety improvement.

3. SIMULATION METHODOLOGY

The simulation methodology is designed to compare the thermal response of an adaptive charging strategy with that of a constant-current baseline under selected electrical and thermal parameter uncertainties. The analysis is conducted using a reduced-order electro-thermal model implemented in Python. Four battery-chemistry configurations—LFP, NMC, NCA, and a projected solid-state configuration—are evaluated using the same simulation duration and ambient-temperature conditions.

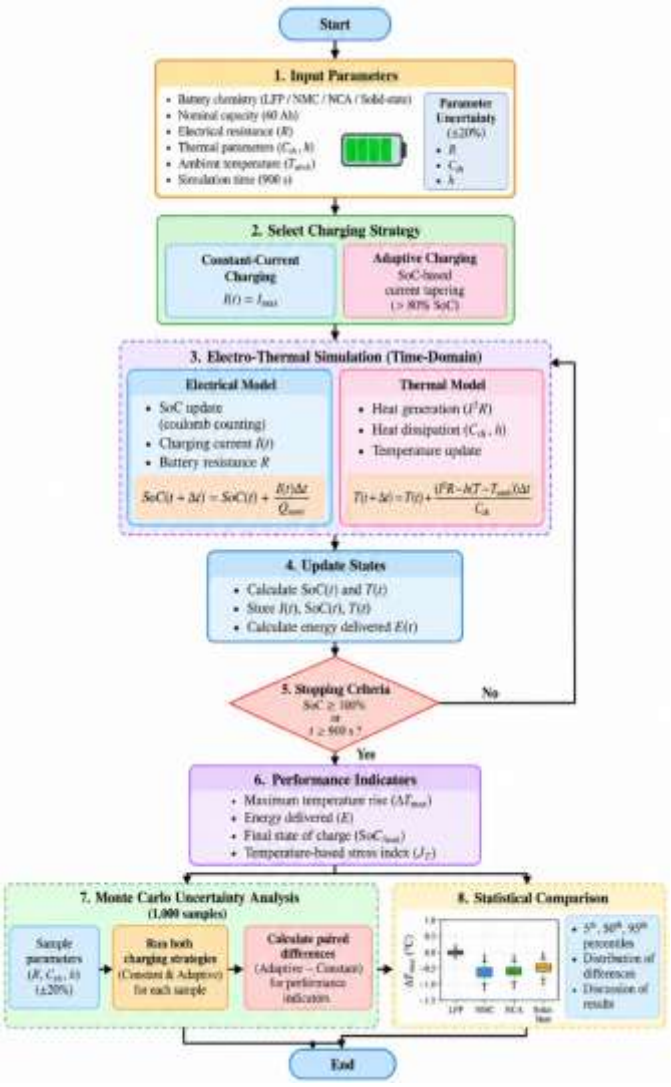


Fig-2: Flowchart of the proposed simulation methodology.

Fig. 2. Flowchart of the proposed electro-thermal simulation framework and Monte Carlo-based uncertainty analysis for comparing constant-current and adaptive charging strategies.

The overall procedure consists of parameter initialization, charging-current calculation, state-of-charge

updating, thermal-response calculation, performance-indicator extraction, and Monte Carlo uncertainty analysis. Both charging strategies are evaluated separately for each parameter sample, with the same sampled electrical resistance, effective thermal capacity, and cooling coefficient applied to both strategies. This paired evaluation helps isolate differences associated with the prescribed charging-current profiles within the assumptions of the model.

The simulation is implemented in Python using NumPy for numerical operations, pandas for data organization, and Matplotlib for generating figures. The charging interval is set to 900 s, with a fixed integration time step of 1 s. The initial state of charge is set to zero, and the initial battery temperature is equal to the ambient temperature of 25°C.

The nominal battery capacity is 60 Ah. Chemistry-dependent resistance values and maximum C-rate limits are assigned according to the parameter set described in Section-2. The model uses an assumed constant pack voltage of 833.3 V, an effective thermal capacity of 20,000 J/K, and a cooling coefficient of 5 W/K. These thermal parameters are modelling assumptions rather than experimentally calibrated values.

A fixed random seed is used to make the Monte Carlo sampling reproducible. The same parameter samples are applied to both charging strategies within each paired comparison.

3.1. Implementation of Charging Strategies

Two charging-current profiles are evaluated.

Constant-current baseline: The charging current is set to the maximum prescribed current for the corresponding battery-chemistry configuration. The current is maintained until the simulated state of charge reaches 100%, after which charging stops. The implementation also limits the final current increment to prevent the state-of-charge calculation from exceeding its upper bound.

Adaptive charging: The maximum prescribed current is applied while the state of charge remains below 80%. Between 80% and 95% SoC, the current decreases linearly toward the assumed terminal current of 1.5C. Beyond 95% SoC, the terminal current is maintained until the model reaches full SoC. Charging is then terminated.

The two strategies are evaluated over the same 15-minute interval. Consequently, their final states of charge and delivered energies may differ. The comparison represents a prescribed adaptive current schedule rather than an optimized controller or a complete constant-current/constant-voltage charging system.

3.2. Time-Domain Simulation

At each simulation time step, the commanded charging current is determined from the selected strategy and the current state of charge. The state of charge is then updated using the discrete coulomb-counting equation. The resulting current is used to calculate resistive heat generation and the heat removed through the effective cooling term.

The battery temperature is updated using the forward Euler discretization. The calculated temperature is constrained not to fall below the ambient temperature. The process is repeated until the simulation reaches the 900 s horizon or the charging process terminates at full state of charge.

For each run, the simulation records the current profile, state-of-charge trajectory, temperature trajectory, approximate energy delivered, maximum temperature rise, and temperature-based stress index. The stress index is calculated and is used only to compare simulated temperature histories; it is not interpreted as a direct measure of electrochemical degradation.

3.3. Monte Carlo Uncertainty Procedure

The uncertainty analysis investigates the sensitivity of the modelled response to variations in three parameters: electrical resistance, effective thermal capacity, and cooling coefficient. Each parameter is independently sampled from a uniform distribution spanning ±20% of its nominal value. A total of 1,000 parameter samples are generated for each chemistry using the fixed random seed.

For every sample, both charging strategies are simulated using identical sampled parameter values. This paired design avoids comparing the adaptive controller under one set of thermal assumptions with the baseline under another set.

The paired difference for each performance indicator is calculated as in Eq. (5)

$$\Delta Y^{(m)} = Y^{(m)}_{\text{adaptive}} - Y^{(m)}_{\text{baseline}} \quad (5)$$

where (m) identifies the Monte Carlo sample. For maximum temperature rise, a negative paired difference indicates that the adaptive strategy produces a lower simulated peak temperature rise for that sample.

The 5^{th}, 50^{th}, and 95^{th} percentiles are extracted to summarize the distribution of each indicator and its paired difference. The fraction of samples with a negative temperature-rise difference is also calculated. These statistics describe the response of the specified model within the selected parameter ranges. They do not represent confidence intervals for actual battery behaviour because the uncertainty distributions have not been calibrated against experimental data.

3.4. Performance Evaluation

The two charging strategies are assessed using four indicators:

1. **Maximum temperature rise:** the maximum simulated battery temperature minus ambient temperature over the charging interval.
2. **Energy delivered:** the approximate electrical energy transferred during the simulation, calculated using the assumed constant pack voltage.

3. **Final state of charge:** the state of charge at the end of the charging interval.
4. **Temperature-based stress index:** the time integral approximated by the discrete sum of squared temperature elevation above ambient.

The indicators are considered together because a lower predicted temperature rise may be accompanied by reduced energy delivery. The final SoC provides additional context for determining whether the adaptive controller's taper region was reached during the simulated interval.

Results are reported separately for each battery-chemistry configuration. The projected solid-state case is treated as a parameter-based scenario rather than as an experimentally established representation of a commercial solid-state battery.

The fixed time step, simulation horizon, parameter definitions, random seed, and Monte Carlo sample count are recorded to support reproducibility. The generated numerical outputs are stored in CSV files, while plots are produced for visual comparison of the charging and thermal responses.

The methodology is intended to quantify differences between two prescribed charging strategies within a simplified electro-thermal model. The analysis does not include experimental calibration, spatial temperature distribution, a detailed battery-voltage model, or an electrochemical degradation model. Accordingly, the results are interpreted as exploratory simulation findings. Numerical convergence and independent validation against measured charging and temperature data remain necessary before extending the conclusions to physical EV battery systems.

4. RESULTS AND DISCUSSION

4.1. Nominal Thermal Performance

The nominal simulation results are used to examine the effect of adaptive charging on the predicted thermal response of the four battery-chemistry configurations. The comparison considers maximum temperature rise, energy delivered during the 15-minute charging interval, and final state of charge. The results are obtained using the reduced-order electro-thermal model and the parameter assumptions described in Sections-2 and 3.

For the NMC configuration, the maximum temperature rise decreases from approximately 5.80°C under constant-current charging to 5.15°C under adaptive charging. This corresponds to a reduction of approximately 0.65°C, or 11.2% relative to the baseline temperature rise. Energy delivered decreases from approximately 50.00 kWh to 46.79 kWh over the same interval as given in Table 2. Thus, under the selected assumptions, the lower predicted temperature rise is accompanied by reduced energy delivery.

Table-2. Nominal simulation results for constant-current and adaptive charging

Battery configuration	Charging strategy	Maximum temperature rise (°C)	Energy delivered (kWh)	Final SoC (%)
LFP	Constant-current	3.92	37.50	75.0
LFP	Adaptive	3.92	37.50	75.0
NMC	Constant-current	5.80	50.00	100.0
NMC	Adaptive	5.15	46.79	93.6
NCA	Constant-current	5.29	50.00	100.0
NCA	Adaptive	4.68	48.81	97.6
Projected solid-state	Constant-current	4.45	50.00	100.0
Projected solid-state	Adaptive	3.93	50.00	100.0

A similar trend is observed for NCA. Its maximum temperature rise decreases from approximately 5.29°C to 4.68°C, corresponding to a reduction of approximately 0.61°C, or 11.5%. The energy delivered decreases from approximately 50.00 kWh to 48.81 kWh. These findings indicate that the effect of the adaptive schedule depends on the prescribed current limit and the state of charge reached during the charging interval.

For the projected solid-state configuration, the predicted maximum temperature rise decreases from approximately 4.45°C to 3.93°C. Both strategies deliver approximately 50.00 kWh in the nominal simulation. This outcome is specific to the assumed parameter set and the selected charging horizon; it does not establish that solid-state batteries inherently provide better thermal performance.

The LFP configuration produces the same maximum temperature rise, energy delivery, and final SoC under both strategies. The final SoC reaches only 75%, which is below the adaptive controller's 80% taper threshold. Consequently, both controllers apply the same current throughout the simulated interval. This result demonstrates that the benefit of an SoC-triggered adaptive strategy depends on whether its control region is reached within the selected charging window.

4.2. Comparison of Adaptive Charging Benefits

To compare the nominal thermal response, the percentage reduction in maximum temperature rise is calculated as in Eq. (6).

$$R_T = \frac{\Delta T_{max,CC} - \Delta T_{max,AD}}{\Delta T_{max,CC}} \times 100 \quad (6)$$

where $(\Delta Tmax, cc)$ and $(\Delta Tmax, AD)$ represent the maximum temperature rises for constant-current and adaptive charging, respectively.

Table -3. Nominal change in maximum temperature rise

Battery configuration	Reduction in temperature rise (°C)	Relative reduction (%)
LFP	0.00	0.0
NMC	0.65	11.2
NCA	0.61	11.5

Projected solid-state	0.52	11.7

The results in Table 3, show that adaptive charging produces a lower nominal maximum temperature rise in three of the four configurations. The relative reductions are approximately 11–12% for NMC, NCA, and the projected solid-state parameter set. However, the absolute temperature differences are less than 1°C in these simulations.

These percentages describe the modelled temperature rise above ambient, not the absolute battery temperature or a measured reduction in battery degradation. They should therefore be interpreted as comparative simulation indicators rather than evidence of improved battery lifetime or safety.

4.3. Paired Monte Carlo Uncertainty Analysis

The nominal results alone do not indicate whether the observed differences persist when model parameters vary. To investigate this issue, paired Monte Carlo simulations are conducted by varying electrical resistance, effective thermal capacity, and cooling coefficient within ±20% of their nominal values are presented in Fig. 3, Fig .4 and Fig. 5. Both charging strategies use the same sampled parameters for each paired comparison are given in Table 4.

For NMC, the median adaptive-minus-baseline difference in maximum temperature rise is approximately −0.65°C. The 5th and 95th percentiles are approximately −0.87°C and −0.49°C, respectively. For NCA, the median paired difference is approximately −0.61°C, with corresponding percentiles of approximately −0.80°C and −0.46°C. For the projected solid-state configuration, the median difference is approximately −0.52°C, with percentiles of approximately −0.68°C and −0.39°C.

Table-4. Paired Monte Carlo differences in maximum temperature rise

Battery configuration	5th percentile (°C)	Median (°C)	95th percentile (°C)
LFP	0.00	0.00	0.00
NMC	−0.87	−0.65	−0.49
NCA	−0.80	−0.61	−0.46
Projected solid-state	−0.68	−0.52	−0.39

For NMC, NCA, and the projected solid-state configuration, the paired temperature-rise difference remains negative across the simulated parameter samples. This indicates that the direction of the thermal response difference is consistent within the selected model, controller design, and uncertainty bounds. In contrast, the LFP difference remains zero because the taper region is not activated during the charging interval.

The result should not be interpreted as a 100% probability that adaptive charging will reduce temperature in a real battery. The Monte Carlo analysis varies only three parameters within prescribed ranges, while retaining the same thermal-model structure and controller. Uncertainty in the model equations, voltage response, initial conditions, battery design, and charging constraints is not fully represented.

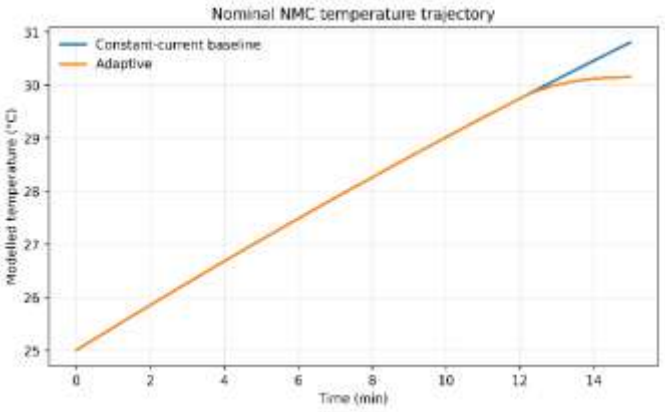


Fig-3: NMC battery temperature profiles under two charging strategies.

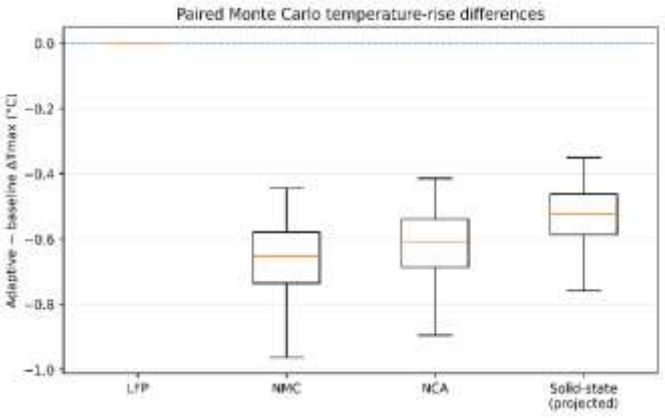


Fig-4: Monte Carlo analysis of temperature-rise differences.

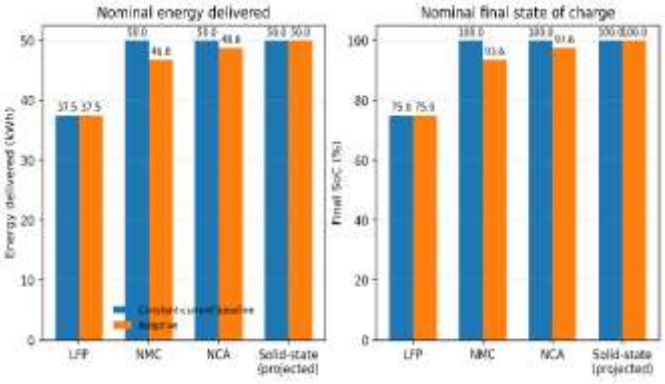


Fig-5: Comparison of energy delivery and final SoC.

4.4. Interpretation of Energy Delivery and State of Charge

The energy-delivery results provide important context for interpreting the thermal differences. For NMC, adaptive charging delivers approximately 3.21 kWh less energy than the baseline during the simulated interval. For NCA, the difference is approximately 1.19 kWh. These differences reflect the prescribed adaptive current schedule and the model's response over a fixed duration.

The final SoC values further explain the comparison. The adaptive NMC case ends at approximately 93.6% SoC, while the constant-current case reaches the model's full-charge limit.

For NCA, adaptive charging reaches approximately 97.6% SoC, compared with 100% for the baseline. These differences indicate that the thermal response cannot be evaluated independently of the amount of charge transferred.

For the projected solid-state case, both strategies reach the full-charge limit within the modelled interval, and the calculated energy values are equal at the displayed precision. This behaviour results from the prescribed current-rate limit and assumed parameters. It should not be interpreted as proof that an adaptive controller can maintain equal energy delivery while reducing temperature in a physical solid-state battery.

The results suggest that a fair charging-strategy comparison should report thermal response, energy delivered, and final SoC together. A strategy that produces a lower peak temperature while delivering less energy may represent a different operating trade-off rather than an unconditional improvement.

4.5. Discussion of the Temperature-Based Stress Index

The temperature-based stress index, defined in (9), summarizes the magnitude and duration of temperature elevation above ambient. It is included to complement the peak-temperature metric because two temperature trajectories can have similar peaks but different durations.

The index should be evaluated using the paired simulation outputs for each chemistry and charging strategy. Lower values indicate a smaller accumulated squared temperature elevation within the definition of the index. However, this mathematical relationship alone does not establish lower electrochemical degradation or longer battery life.

Because the present model does not include a validated aging equation, capacity-fade data, or an experimentally established relationship between temperature history and degradation, the index is used only as a thermal-response comparison measure. Any claim of reduced degradation would require additional evidence and an appropriate degradation model.

4.6. Limitations and Implications

Several limitations affect the interpretation of the results. First, the battery resistance, effective thermal capacity, cooling coefficient, and chemistry-specific C-rate limits are prescribed inputs rather than parameters calibrated against a common experimental dataset. Second, the constant pack-voltage assumption simplifies the calculation of energy delivered and does not represent the voltage evolution of a practical battery during charging. Third, the lumped thermal model excludes spatial temperature gradients and several electrochemical heat-generation mechanisms. Fourth, the uncertainty bounds are exploratory and have not been derived from measured parameter distributions.

The projected solid-state configuration introduces an additional limitation because its parameter set does not represent experimentally validated behaviour for a specific commercial battery. Furthermore, the current controller is a prescribed SoC-dependent taper, not an optimized charging algorithm subject to a complete set of practical battery-management constraints.

Within these limitations, the simulations demonstrate that adaptive current scheduling can change the predicted thermal response, and that the magnitude of the difference depends on the chemistry-specific assumptions and whether the taper threshold is reached. The paired Monte Carlo analysis adds evidence about sensitivity to the selected parameter variations, but it does not replace calibration or independent validation.

Future work should incorporate a consistent pack-level electrical representation, experimentally informed thermal parameters, a voltage-versus-SoC model, and independent temperature measurements. A validated degradation model would also be necessary before evaluating effects on capacity fade or battery lifetime. These extensions would help determine whether the trends observed in the present exploratory simulations persist under more realistic operating conditions.

5. CONCLUSION

This paper investigated the simulated thermal response of an adaptive charging strategy compared with a constant-current baseline for four electric vehicle battery-chemistry configurations. A reduced-order electro-thermal model was implemented to evaluate maximum temperature rise, energy delivered, final state of charge, and a temperature-based stress index over a 15-minute charging interval. A paired Monte Carlo procedure was also considered to examine the sensitivity of the predicted response to variations in electrical resistance, effective thermal capacity, and cooling coefficient. Under the selected nominal model assumptions, adaptive charging reduced the predicted maximum temperature rise for the NMC, NCA, and projected solid-state configurations. For NMC, the maximum temperature rise decreased from approximately 5.80°C to 5.15°C, whereas for NCA it decreased from approximately 5.29°C to 4.68°C. These reductions were accompanied by differences in energy delivery during the fixed charging interval. In contrast, the LFP configuration exhibited no difference between the charging strategies because its simulated state of charge remained below the adaptive controller's activation threshold. The paired uncertainty analysis further indicated that the direction of the predicted thermal-response difference remained consistent for NMC, NCA, and the projected solid-state configuration within the selected parameter ranges. This finding is conditional on the prescribed controller, simplified model structure, and assumed uncertainty distributions. It should not be interpreted as a probability of improved performance in a physical battery system. The principal outcome of this investigation is that the predicted effect of adaptive charging depends on the current-control schedule, charging duration, and assumed electrical and thermal parameters. Reporting temperature rise together with energy delivery and final state of charge provides a more informative comparison than relying on a single thermal indicator. The temperature-based stress index offers an additional means of comparing simulated temperature trajectories, but it does not directly quantify capacity fade or battery lifetime. The present work is exploratory and simulation-based. The model has not been calibrated against experimental measurements, and its

constant-voltage approximation and lumped thermal representation limit its physical accuracy. Consequently, the results should be interpreted as comparative numerical observations rather than validated claims concerning battery safety, degradation reduction, or service-life improvement.

REFERENCES

[1] K. Kumar, P. Ramji Tiwari, P. Venkata Varaprasad, C. Babu, and K. Jyotheeswara Reddy, "Performance evaluation of fuel cell fed electric vehicle system with reconfigured quadratic boost converter," International Journal of Hydrogen Energy, vol. 46, no. 11, pp. 8167–8178, 2021.

[2] A. Tomaszewska et al., "Lithium-ion battery fast charging: A review," eTransportation, vol. 1, Art. no. 100011, 2019.

[3] P. Makeen, H. A. Ghali, and S. Memon, "A review of various fast charging power and thermal protocols for electric vehicles represented by lithium-ion battery systems," Future Transportation, vol. 2, no. 1, pp. 281–299, 2022.

[4] Y. Zeng et al., "Extreme fast charging of commercial Li-ion batteries via combined thermal switching and self-heating approaches," Nature Communications, vol. 14, Art. no. 3229, 2023.

[5] S. Jarid and M. Das, "An electro-thermal model based fast optimal charging strategy for Li-ion batteries," AIMS Energy, vol. 9, no. 5, pp. 915–933, 2021.

[6] G. Chen, Z. Liu, and H. Su, "An optimal fast-charging strategy for lithium-ion batteries via an electrochemical–thermal model with intercalation-induced stresses and film growth," Energies, vol. 13, no. 9, Art. no. 2388, 2020.

[7] P. Nambisan, P. Saha, and M. Khanra, "Real-time optimal fast charging of Li-ion batteries with varying temperature and charging behaviour constraints," Journal of Energy Storage, vol. 41, Art. no. 102918, 2021.

[8] X. Lin, H. E. Perez, S. Mohan, J. B. Siegel, A. G. Stefanopoulou, Y. Ding, and M. P. Castanier, "A lumped-parameter electro-thermal model for cylindrical batteries," Journal of Power Sources, vol. 257, pp. 1–11, 2014.

[9] C. Zou, X. Hu, Z. Wei, and X. Tang, "Electrothermal dynamics-conscious lithium-ion battery cell-level charging management via state-monitored predictive control," Energy, vol. 141, pp. 250–259, 2017.

[10] L. Mattia, H. Beiranvand, W. Zamboni, and M. Liserre, "Lithium-ion battery thermal modelling and characterisation: A comprehensive review," Journal of Energy Storage, vol. 129, Art. no. 117114, 2025.

[11] K. Kumar, V. Lakshmi Devi, P. Avagaddi, and K. Murali Kumar, "Design and evaluation of power converter for integration of lithium-ion battery and renewable sources," Results in Engineering, vol. 25, Art. no. 104409, 2025.

[12] K. Kumar, V. Lakshmi Devi, C. Dhanamjayulu, H. Kotb, and A. Elrashidi, "Evaluation and deployment of a unified MPPT controller for hybrid Luo converter in combined PV and wind energy systems," Scientific Reports, vol. 14, Art. no. 3248, 2024.

[13] F. S. Hwang, T. Confrey, C. Reidy, D. Picovici, D. Callaghan, D. Culliton, and C. Nolan, "Review of battery thermal management systems in electric vehicles," Renewable and Sustainable Energy Reviews, vol. 192, Art. no. 114171, 2024.

[14] L. D. Tai, K. S. Garud, S.-G. Hwang, and M.-Y. Lee, "A review on advanced battery thermal management systems for fast charging in electric vehicles," Batteries, vol. 10, no. 10, Art. no. 372, 2024.

[15] G. L. Plett, "Extended Kalman filtering for battery management systems of LiPB-based HEV battery packs," Journal of Power Sources, 2004.